Preliminary Communication

For reprint orders, please contact: reprints@futuremedicine.com

Nanomedicine

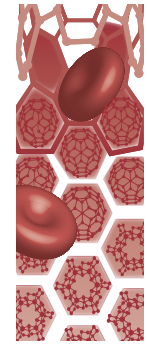

Differentiation of reactive-like astrocytes cultured on nanofibrillar and comparative culture surfaces

Aim: To investigate the directive importance of nanophysical properties on the morphological and protein expression responses of dibutyryladenosine cyclic monophosphate (dBcAMP)-treated cerebral cortical astrocytes *in vitro*. **Materials & methods:** Elasticity and work of adhesion characterizations of culture surfaces were performed using atomic force microscopy and combined with previous surface roughness and polarity results. The morphological and biochemical differentiation of dBcAMP-treated astrocytes cultured on promising nanofibrillar scaffolds and comparative culture surfaces were investigated by immunocytochemistry, colocalization, super resolution microscopy and atomic force microscopy. The dBcAMP-treated astrocyte responses were further compared with untreated astrocyte responses. **Results & conclusion:** Nanofibrillar scaffold properties were shown to reduce immunoreactivity responses while poly-l-lysine-functionalized Aclar® (Ted Pella Inc., CA, USA) properties were shown to induce responses reminiscent of glial scar formation. The comparison study indicated that directive cues may differ in wound-healing versus quiescent situations.

Keywords: astrocyte morphology • atomic force microscopy • confocal microscopy • elasticity • immunoreactivity • nanofibrillar scaffolds • surface energy

Volkan Müjdat Tiryaki*[,1], Virginia M Ayres[1], Ijaz Ahmed[2] & David I Shreiber[2]

[1]Electronic & Biological Nanostructures Laboratory, Department of Electrical and Computer Engineering, 428 S Shaw Lane, Michigan State University, Engineering Building Room 2120, East Lansing, MI, 48824, USA

[2]Department of Biomedical Engineering, Rutgers, The State University of New Jersey, 599 Taylor Road, Piscataway, NJ 08854, USA

*Author for correspondence:
Tel.: +1 517 432 1972
Fax: +1 517 353 1980
tiryakiv@msu.edu

Repair of traumatic injury to the CNS remains a challenging problem. One of the hurdles that must be overcome is the glial scar, which is established after traumatic injury in mammalian systems and creates a barrier to regeneration of axons [1,2]. A glial scar consists mainly of reactive astrocytes and proteoglycans. Reactive astrocytes at a wound site undergo a morphological change, extending interwoven processes that form chain-like clusters [3]. Furthermore, they express tenascins [4], and inhibitory chondroitin (C)- and keratan (K)-sulfate proteoglycans [5]. The glial scar biomechanically and biochemically blocks axonal elongation and reconnection [6].

Recent research by our group has identified an implantable scaffold composed of electrospun polyamide nanofibers that appears to have promising wound-healing properties for CNS neural cell systems, including mitigation of astrocytic scarring. *In vivo*, when the scaffolds were introduced into spinal cord wound sites (rat model) accelerated hindlimb recovery, measured by standardized observational scoring (Beattie, Basso, Breshnahan [BBB] score), was observed, with aligned and fasciculated axon development and revascularization throughout wound sites [7,8]. Moreover, low levels of astrocytic scarring were observed at 3 and 5 weeks after injury in comparison to injury-only controls [7]. The promising *in vivo* results motivated a series of further *in vitro* investigations. Results from our group and from other groups have demonstrated that electrospun nanofibrillar scaffolds encourage biomimetic astrocyte stellation [9–11], glial fibrillary acidic protein (GFAP) down-regulation [10,11], growth factor upregulation [9] and neurite outgrowth by cocultured neurons [9]. Therefore, *in vitro* studies also

Future Medicine part of fsg

indicate that nanofibrillar scaffolds hold potential for CNS regenerative medicine.

Determination of how the physical properties of the nanofibrillar scaffolds influence the morphological and protein expressions is under investigation by our group and other groups. The effect of a physical environment on cell adhesion and differentiation has recently been recognized, especially in neural cells. Collectively, studies of cell responses to nano-patterning [12–17], elasticity [18–23], surface roughness [12,24,25] and surface polarity [12,26] suggest that controlling aspects of the physical environment holds potential for inducing preferential differentiation of reactive astrocytes into noninhibitory pathways. This potential, combined with the promising *in vitro* and *in vivo* results, motivated the present investigation of dibutyryladenosine cyclic monophosphate (dBcAMP)-treated astrocyte differentiation in response to the external physical cues provided by the nanofibrillar scaffolds.

Cerebral cortical astrocytes, a relatively uniform population, were treated with dBcAMP, and used to investigate the responses of reactive-like astrocytes to external physical cues. Astrocytes treated with dBcAMP develop morphologies that resemble the reactive astrocytes [27]. As only external cues were used to trigger cell responses, astrocyte responses to nanofibrillar surfaces were studied in comparison with their responses to three additional culture surfaces: poly-L-lysine-functionalized planar glass (PLL glass), unfunctionalized planar Aclar (Aclar®, Ted Pella Inc., CA, USA), and PLL-functionalized planar Aclar (PLL Aclar). PLL glass is a standard astrocyte culture surface, and astrocyte responses to it are well characterized, making it useful for identifying differences in astrocyte responses to other surfaces. The polyamide nanofibrillar scaffolds were electrospun on Aclar substrates; therefore, astrocyte responses to Aclar surfaces were investigated to distinguish responses to the nanofibrillar scaffolds from possible responses to the underlying Aclar substrate, particularly with respect to the elasticity property. Astrocyte responses to PLL Aclar surfaces were studied to clarify the role of the underlying substrate versus surface functionalization, particularly with respect to the elasticity and surface polarity properties. As these were the same comparative culture surfaces used in our recent investigation of untreated cerebral cortical astrocytes responses to external physical cues [12], investigations of the differences between the untreated and dBcAMP-treated astrocyte responses to the same culture environments and properties were also performed.

In the present study, the local elasticity and work of adhesion of culture surfaces were investigated using atomic force microscopy (AFM) force curves and the results were added to the previous investigations of surface polarity and surface roughness. Reactive protein expressions for GFAP and tubulin, and chondroitin sulfate proteoglycan (CSPG), a neurite outgrowth-inhibitory proteoglycan, were investigated for dBcAMP-treated and untreated astrocytes. Cytoskeletal protein expressions for the Rho GTPases Cdc42 (filopodia), Rac1 (lamellipodia) and RhoA (elevated: stress fibers and depressed: stellation) were investigated for the dBcAMP-treated astrocytes and the results were compared with previous results [12] for untreated astrocytes. The physical property trends were compared with the morphological and protein expression responses. The present work continues to explore the hypothesis that external physical cues of the nanofibrillar scaffolds can trigger the initiation of specific signaling cascades with morphological and reactivity consequences.

The morphological responses of cerebral cortical astrocytes were investigated at high-resolution using AFM and super-resolution microscopy (SRM). The three dimensional capability of AFM was also used to characterize cell spreading. The studies of the corresponding activations of the reactive proteins GFAP and tubulin, and the inhibitory proteoglycan CSPG, were performed using immunocytochemistry. GFAP, tubulin and CSPG expressions are associated with the astrocytic scarring response. Additionally, Rho GTPase proteins associated with morphological responses were investigated. Quantification of protein expressions were performed using confocal laser scanning microscopy (CLSM) z-series.

This article is organized as follows. Investigations of the physical properties of each culture environment, assessed in terms of local elasticity, work of adhesion, RMS surface roughness, and surface polarity, are presented first. The results indicated that the culture surfaces presented statistically significant property differences to astrocytes. Investigations of the astrocyte responses, assessed in terms of morphology and protein expressions, are presented next. Quantitative measures of the morphological responses for dBcAMP-treated astrocytes were compared with those of untreated astrocytes [12]. All of the protein expression investigations were performed for untreated and dBcAMP-treated astrocytes, with comparison of results.

One important finding of the present study was that dBcAMP-treated astrocytes cultured on nanofibrillar scaffolds showed a unique non-response, meaning that the reactivity proteins GFAP and tubulin, inhibitory proteoglycan CSPG, and cytoskeletal Rho GTPase expressions were little changed from their untreated expressions. A second important finding was that dBcAMP-treated astrocytes cultured on the PLL Aclar surfaces exhibited responses that were reminiscent of glial scar formation.

The comparison of dBcAMP-treated and untreated astrocyte responses suggested that different nanophysical cues may have more directive importance in a wound-healing situation. The elasticity property was indicated as potentially more directive for dBcAMP-treated astrocytes than for untreated astrocytes.

Materials & methods

Nanofibrillar scaffolds & comparative culture surfaces

Nanofibrillar scaffolds and comparative culture surfaces: PLL glass, PLL Aclar and Aclar were supplied/prepared as described in [12]. Scanning electron microscope (SEM) images (not shown) confirmed uniform coverage of nanofibers with no exposure of the Aclar coverslips. The culture surfaces used for the physical properties investigations were immersed in culture media only (no cells) for 24 h followed by fixative wash and dry.

Primary untreated & dBcAMP-treated astrocyte cultures

Primary untreated astrocyte culture preparation was identical to our previous work [12]. Primary dBcAMP-treated astrocyte culture preparation was as follows [27,28]. Cerebral hemispheres of new born Sprague Dawley rats (postnatal day 1 or 2) were isolated aseptically. Cerebral cortices were dissected out, freed of meninges, and collected in HBSS. They were minced with sterile scissors and digested in 0.1% trypsin and 0.02% DNase for 20 min at 37°C. The softened tissue clumps were then triturated by passing several times through a fine bore glass pipette to obtain a cell suspension. The cell suspension was washed twice with culture media (DMEM + 10% FBS) and filtered through a 40-µm nylon mesh. For culturing, the cell suspension was placed in 75-cm^2 flasks (one brain/flask in 10 ml growth medium) and incubated at 37°C in a humidified CO_2 incubator. After 3 days of incubation the growth media was removed, cell debris was washed off and fresh medium was added. The medium was changed every 3–4 days. After reaching confluency (~7 days), the cultures were shaken to remove macrophages and other loosely adherent cells. To obtain reactive-like astrocytes, 0.25 mM dBcAMP was added to the culture medium and the serum concentration was reduced to 1%. The cultures in dBcAMP containing medium were incubated for 7–8 more days with a media change every 3–4 days. The morphology of the cells was observed on alternate days under a phase contrast microscope. In the control cultures, the cells were fed with DMEM + 1% FBS (without dBcAMP). All procedures were approved by the Rutgers Animal Care and Facilities Committee (IACUC Protocol #02–004).

After completing dBcAMP treatment, reactive-like astrocytes were then harvested with 0.25% Trypsin/EDTA (Sigma-Aldrich) and re-seeded at a density of 30,000 cells per well directly on 12-mm Aclar or PLL Aclar coverslips, PLL glass coverslips, or on Aclar coverslips coated with nanofibers in 24-well plates in astrocyte medium containing dBcAMP (0.5 ml). After culturing the dBcAMP-treated astrocytes on the aforementioned substrates for 24 h, they were fixed with paraformaldehyde. Parallel cultures were immunostained with GFAP, an identification marker for astrocytes, and more than 95% were found to be GFAP-positive.

Astrocyte density measurement

The dBcAMP-treated astrocyte density on different cell substrates was measured by counting the nuclei from 22 DAPI (Life Technologies) immunofluorescence images per culture surface. Untreated astrocyte density was measured by counting cells from 22 GFAP and CSPG immunofluorescence images. Each image contained approximately 15–30 cells.

AFM

AFM images of astrocytes were captured using a Veeco Instruments Nanoscope IIIA (Bruker AXS Inc., WI, USA; formerly Veeco Metrology) operated in ambient air. A J scanner with 125 µm × 125 µm × 5.548 µm x–y–z scan range was used. The AFM was operated in contact mode silicon nitride tips with a nominal tip radius of 25 nm and cantilever spring constant k = 0.58 N/m (Nanoprobe SPM tips, Bruker AXS Inc.; formerly Veeco Metrology). Frequency domain Gaussian high pass filtering (GHPF) was used to segment the astrocytes from the substrate backgrounds in AFM height images [29].

Astrocytes cultures prepared for AFM imaging were unstained. Four samples of astrocytes on each substrate were prepared. The uniformity of the four samples on each substrate was assessed by phase contrast microscopy to ensure that the cultures were representative. AFM images of at least 20 astrocytes for each culture surface were evaluated for process length, soma height, and cell shape index (CSI). Variations in astrocyte process length, soma height and CSI data among the culture surfaces were analyzed using ANOVA followed by pairwise *post hoc* comparisons with Tukey's test [30]. Significance levels were set at $p < 0.05$.

Astrocyte process length measurement

Untreated and dBcAMP-treated astrocyte cell process lengths were measured based on GHPF [29] AFM height images. An extension longer than the diameter of a cell soma was considered to be a process.

10.2217/NNM.14.33

Astrocyte soma height measurement

Untreated and dBcAMP-treated astrocyte maximum soma height values were measured using the section analysis of Nanoscope Software version 5.30r3.sr3 and NanoScope Analysis 1.10 (Bruker AXS Inc.; formerly Veeco Metrology).

Astrocyte cell shape index

The CSI was defined as the ratio of the perimeter squared to the two-dimensional cell area [31]:

$$CSI = \frac{P^2}{2\pi A} \quad \text{(Equation 1)}$$

Where P is the cell perimeter and A is the cell area. This definition describes stellation as a departure from $CSI = 1$ for a circular cell [32,33]. The cell perimeter and area were calculated following manual segmentation of cells from GHPF AFM height images. The procedure was implemented in MATLAB version 7.7.0 (R2008b) Image Processing Toolbox (The MathWorks Inc., MA, USA).

AFM force curves of culture surfaces

Twenty force versus z-piezo displacement curves from each culture surfaces were collected using the force mode analysis in Nanoscope Software version 5.30r3.sr3. The deflection sensitivity was determined on a silicon wafer, which is known to be harder than the culture surfaces [34]. The force versus z-piezo displacement data was converted to force versus distance (F–d) curve. Using the cantilever stiffness of the AFM provided by the manufacturer (0.6 N/m), the elasticity of tissue cultures was calculated from the retraction curve according to the Derjaguin, Muller and Toporov (DMT) model [35]:

$$\delta = \frac{a^2}{R} \quad \text{(Equation 2)}$$

$$a = \left((F_n + F_{ad})\frac{R}{K}\right)^{1/3} \quad \text{(Equation 3)}$$

$$F_{ad} = 2\pi W_{132} R \quad \text{(Equation 4)}$$

$$\frac{1}{K} = \frac{3}{4}\left(\frac{1-\upsilon_{tip}^2}{E_{tip}} + \frac{1-\upsilon_{sample}^2}{E_{sample}}\right) \quad \text{(Equation 5)}$$

Where δ is the indentation, a is the contact radius, R is the tip radius, F_n is the applied force, F_{ad} is the adhesion force, K is the total elastic modulus of the tip-substrate, W_{132} is the work of adhesion required to separate AFM tip (subscript $_2$) from cell substrate (subscript $_1$) in air (subscript $_3$) [36], ν_{tip} is the Poisson's ratio of silicon nitride AFM tip, ν_{sample} is the Poisson's ratio for sample, E_{tip} is the Young's modulus of silicon nitride AFM tip set, and E_{sample} is the Young's modulus of sample. The AFM tip radius was measured to be 51 nm using field emission SEM images (not shown). F_n was limited to approximately 25 nN by using the relative trigger threshold mode in the Nanoscope software. Poisson's ratio values ν equal to 0.27 for silicon nitride [37], 0.39 for polyamide [38], 0.22 for glass [39], and 0.33 for Aclar [40] were used. E_{tip} was set equal to 310 GPa [37] and E_{sample} was calculated by using a least-squares fit of F–d curves to the DMT model, and implemented using the MATLAB lsqcurvefit command [41]. The adhesive component of the AFM force curves was extracted, and used to investigate the work of adhesion between the AFM tip and the culture surfaces. Variations in elasticity and work of adhesion data among the culture surfaces were analyzed using ANOVA followed by pairwise *post hoc* comparisons with Tukey's test [30]. Significance levels were set at $p < 0.05$.

Immunolabeling for GFAP & tubulin

Astrocytes cultured on coverslips were fixed with 4% paraformaldehyde for 10 min, permeabilized with 0.5% Triton X-100 in PBS for 5 min, and blocked with 10% normal goat serum for 30 min. After removing the normal goat serum, the cells were double stained with one of the primary antibodies and phalloidin. Rabbit anti-GFAP (Dako, CA, USA) was diluted 1:500 while mouse anti-β-tubulin (Sigma-Aldrich, MO, USA) was diluted 1:200. The incubation in the primary antibodies was done overnight at room temperature in a humidity chamber. Coverslips were then washed three times with PBS and stained appropriate secondary antibody either goat anti-rabbit Alexa 568 IgG (Life Technologies, CA, USA) or goat anti-mouse Alexa 568 IgG (Life Technologies). Both secondary antibodies were diluted 1:500 and incubation was for 1 h at room temperature. Secondary antibody staining coverslips were rinsed three times with PBS. Following PBS rinse, the coverslips were stained with Alexa Fluor® 488 Phalloidin (Life Technologies) diluted 1:100 for 1 h, rinsed again with PBS as above. After staining, coverslips were mounted on microscopic slides with GelMount (Biomeda, CA, USA), and observed under an Olympus FluoView 1000 Laser Scanning Confocal Microscope system attached to an Olympus IX81 automated inverted microscope platform.

Quantitative GFAP & tubulin expression estimate

A special data acquisition protocol was designed for the protein quantification studies using CLSM. First, immunofluorescence slides were always kept in dark.

Any sample that was exposed to visible light was discarded and not used for protein quantification analysis. Confocal z-series images were captured using an Olympus FluoView 1000 CLSM system attached to an Olympus IX81 automated inverted microscope platform equipped with a 40× oil immersion objective (NA = 1.3). The z-series were acquired under identical imaging conditions, including the same high voltage, offset and gain settings, same objective, and same resolution (1024 × 1024 pixels). The intensity data were collected from samples in three dimensions. The z-step size was set to a level such that the intensity from a fluorophore was only recorded once, and determined by considering the axial resolution of the microscope system. The axial resolution is defined as [42]:

$$AR = 1.4\lambda_{em}/NA^2 \quad \text{(Equation 6)}$$

Where AR = axial resolution, λ_{em} is the emission wavelength, and NA is the numerical aperture of the objective. In these experiments, the maximum λ_{em} was 576 nm, NA was 1.3, and AR was equal to 477 nm. The z-step size was set to 1.13 µm to avoid oversampling. The upper and lower focal planes were determined with care as planes of complete darkness above and below any cell. The maximum pixel intensity was set to a level so that none of the pixels were saturated. This was important for both accuracy of quantification and reduction of photobleaching.

Images were analyzed using MATLAB version 7.7.0 (R2008b) Image Processing Toolbox (The MathWorks) and ImageJ version 1.46r (National Institutes of Health). The maximum intensity projection images were obtained from the z-series, the boundaries of the cells were determined manually, and then the total intensity and the number pixels were calculated by using the z-series and cell boundaries. The cell segmentation was done manually to avoid any error from the software settings since currently there is no robust algorithm for image segmentation. The background intensity was also calculated from slides in three dimensions. The average background intensity values were calculated for each z-series because the autofluorescence was different on different culture surfaces. The average background intensity was then multiplied by the number of pixels of z-series, and subtracted from the total intensity. Finally, the total amount of GFAP or tubulin expression/cell was determined. At least 50 cells were analyzed for each culture surface. Variations in GFAP and tubulin expression estimation data among the culture surfaces were analyzed using ANOVA followed by pairwise *post hoc* comparisons with Tukey's test [30]. Significance levels were set at $p < 0.05$.

Colocalization of GFAP & tubulin

Colocalization analysis was based on three-dimensional z-series GFAP and tubulin immunofluorescence images of ten different regions per each culture. All images had 12 bit gray level depth and 1024 × 1024 pixels. Olympus software FV10-ASW, version 03.01.02.02 (Olympus) was used for the colocalization analysis. The threshold was set manually to a level that minimized background noise. The codependence of GFAP and tubulin expression of untreated and dBcAMP-treated astrocytes was quantitatively investigated by calculating the Pearson's correlation coefficient and the overlap of GFAP and tubulin was quantitatively investigated by calculating the Mander's coefficients M1 and M2 [12,42]. M1 shows the portion of the tubulin intensity that coincides with some intensity in the GFAP image, and M2 shows the reverse. Variations in Pearson correlation coefficient (PC), M1 and M2 among the culture surfaces were analyzed using ANOVA followed by pairwise *post hoc* comparisons with Tukey's test [30]. Significance levels were set at $p < 0.05$.

Quantitative CSPG expression estimate

Astrocytes cultured on coverslips of four different substrates were fixed with 4% paraformaldehyde for 10 min, permeabilized with 0.5% Triton X-100 in PBS for 5 min, and blocked with 10% normal goat serum for 30 min. After removing the normal goat serum, cells were stained overnight at room temperature in a humidity chamber with monoclonal anti-chondrotin sulfate IGM antibody (Sigma-Aldrich) diluted 1:200. Coverslips were then washed three times with PBS and stained for 1 h with Alexa 488 goat anti-mouse IgM secondary antibody (Life Technologies) diluted 1:500. After secondary antibody incubation the coverslips were rinsed three times with PBS and mounted on microscopic slides with GelMount (Biomeda) and observed under a fluorescence microscope.

The 24-h untreated and dBcAMP-treated astrocyte cultures were used for CSPG quantification. Twelve images were captured from each substrate under identical imaging conditions: 1024 × 1024 pixels, 40× oil objective, same high voltage, gain and offset. The high voltage and offset levels were set to a level so that the pixels were not saturated. Total CSPG intensities of culture surfaces were analyzed using MATLAB version 7.7.0 (R2008b) Image Processing Toolbox (The MathWorks).

Three different sets of control cultures were prepared to ensure the accuracy of the quantification. In the first set, the autofluorescence of primary antibody was measured. Its intensity level was shown to be ignorable. In the second set, the nonspecific binding of the secondary antibody was measured, and the intensity measurements

10.2217/NNM.14.33

showed this was also ignorable. In the final control set, cell substrates were treated with primary and secondary antibodies without culturing cells to check if the primary antibody binds to the substrate. As intensities were different on different substrates, each of them was subtracted from the corresponding CSPG intensity. The total CSPG intensity data was then measured. Variations in CSPG expression estimation data among the culture surfaces were analyzed using ANOVA followed by pairwise *post hoc* comparisons with Tukey's test [30]. Significance levels were set at $p < 0.05$.

Quantitative Cdc42, Rac1 & RhoA expression estimate

The dBcAMP-treated astrocytes cultured on the substrates were fixed with 4% paraformaldehyde for 10 min, permeabilized with 0.5% Triton X-100 for 5 min, and blocked with 10% normal goat serum for 30 min. The immunolabeling for Cdc42, Rac1 and RhoA, and the maximum intensity level image capture conditions, were identical to those described in our previous work for untreated astrocytes [12] to enable comparison of results. A total of 240 dBcAMP-treated astrocytes were investigated. Variations in Rho GTPase expression estimation data among the culture surfaces were then analyzed using ANOVA followed by pairwise *post hoc* comparisons with Tukey's test. Significance levels were set at $p < 0.05$.

Results

Physical properties of culture environments

Local elasticity & surface energy investigation

Reported investigations [18–20] have identified local elasticity as potentially directive. Local elasticity along individual nanofibers was characterized in the present work. All force curves exhibited characteristics of interaction with a relatively firm material with an adhesive component and were therefore interpreted using the DMT elasticity interpretative model for the Young's modulus that included adhesion forces [43].

Analysis of the Young's modulus results using median-value box plots (Figure 1A) indicated that PLL glass surfaces presented the hardest and nanofibrillar scaffolds presented the softest culture environments to astrocytes. The Young's moduli for Aclar and PLL Aclar were similar to each other, and higher in value to those of the nanofibrillar scaffolds. The results indicated that substrate elasticity dominated over the PLL chemical functionalization effect since unfunctionalized and PLL functionalized Aclar had similar elasticity median and variances while PLL functionalized glass and PLL functionalized Aclar had different results for both.

Use of the DMT interpretive model further enabled investigation of the surface energies of the cell substrates by measuring the work of adhesion, W_{132}, between the AFM tip and each culture surface [36]. Analysis of the work of adhesion using median-value box plots (Figure 1B) showed that despite the similar functionalization of PLL glass and PLL Aclar, the work of adhesion median value was higher for PLL Aclar. The combination of chemical functionalization with surface roughness may result in higher work of adhesion, possibly through PLL conformation changes. The highest variance was observed for nanofibrillar scaffolds.

The nanoscopic elasticity, work of adhesion, and surface roughness [12], and the macroscopic surface polarity measured by contact angle [12] of culture surfaces, are summarized as mean values with standard error of the mean (SE) in Figure 2. The work of adhesion and contact angle can be both used for measuring surface energy. Surface energy increases as work of adhesion increases, and work of adhesion decreases as contact angle increases. Therefore, the work of adhesion and the contact angle measurements are consistent (Figures 2B & 2D).

Astrocyte responses: morphology investigation

Cell density

The initial cell plating density on all surfaces was 66 cells/mm^2. Astrocyte density at 24 h was measured and the results for untreated and dBcAMP-treated astrocytes for each substrate are given in Table 1.

Astrocyte density can be influenced by many factors. The dBcAMP-treated astrocyte density on Aclar was low compared with other substrates, indicating that the cell adhesion and/or proliferation on Aclar surfaces were negatively influenced by the properties of this substrate. The highest dBcAMP-treated astrocyte cell density was observed on the nanofibrillar scaffolds, which indicated that these surfaces were able to modulate cell adhesion and/or proliferation without requiring PLL functionalization.

Astrocyte morphology investigation by AFM & SRM

The morphological responses and astrocyte–astrocyte interactions of the dBcAMP-treated astrocytes were investigated in detail using AFM and SRM. Astrocytes on all surfaces except PLL Aclar developed interactions via long processes that suggested contact spacing [44]. Extensive nanoscale process formation was also observed for the astrocytes cultured on PLL glass surfaces (Figure 3A). The nanoscale processes were about approximately 10–50 nm in diameter and were observed around both main processes and somata. The astrocytes cultured on nanofibrillar scaffolds typically developed multiple processes in a stellate pattern (Figure 3B). Astrocytes cultured on Aclar

surfaces developed directional processes (Figure 3C). Astrocyte–astrocyte interactions were few in number; when present, they were suggestive of contact spacing. Astrocytes on PLL Aclar also developed long processes, but astrocyte interactions consisted of intertwined processes rather than contact spacing. This resulted in chain-like cell clusters reminiscent of glial scar formation (Figure 3D).

Astrocyte quantitative morphology assessment

The morphological responses for the dBcAMP-treated and untreated astrocytes were quantified using process length, maximum soma heights, and CSI measurements taken from the AFM height images. Pairwise comparisons were made for the dBcAMP-treated astrocytes, untreated astrocytes, and dBcAMP-treated versus untreated astrocytes cultured on the same four culture surfaces. The results (Figure 4) are displayed as mean-value bar graphs with ±SE.

Analysis of the process length (Figure 4A) was performed to investigate stellation and reactivity. The dBcAMP-treatment induced significant increase in process length of astrocytes on all cultures surfaces except nanofibrillar scaffolds. Analysis of astrocyte maximum soma heights (Figure 4B) performed to investigate cell spreading behavior indicated that one effect of dBcAMP-treatment was increased uniformity of cell spreading. Analysis of the two-dimensional CSI (Figure 4C) was performed to investigate stellation. The most significant CSI change was observed for dBcAMP-treated versus untreated astrocytes cultured on PLL Aclar ($p = 0.0037$).

Astrocyte responses

GFAP & tubulin quantification

The total GFAP and tubulin expression of untreated and dBcAMP-treated astrocytes was investigated by confocal z-series. A two-way ANOVA revealed that both the substrate ($p < 0.05$) and dBcAMP treatment had significant effects on GFAP (Figure 5A) and tubulin (Figure 5B) intensity. GFAP and tubulin expressions of the dBcAMP-treated astrocytes were higher than those of their untreated counterparts for all culture surfaces. The dBcAMP-treated astrocytes cultured on nanofibrillar scaffolds had significantly lower expression of GFAP than PLL Aclar and Aclar, and lower expression of tubulin than Aclar. The dBcAMP-treated astrocytes cultured on Aclar had highest expressions of both GFAP and tubulin.

GFAP & tubulin staining & colocalization

Representative GFAP and tubulin staining images of dBcAMP-treated astrocytes are shown in Figure 6. The observed astrocyte-astrocyte interactions differed significantly as a function of culture surfaces and cell density. The dBcAMP-treated astrocytes cultured on PLL glass, nanofibrillar scaffolds, and Aclar surfaces were typically not clustered, while the dBcAMP-treated astrocytes on the PLL Aclar surfaces (Figure 6) displayed pronounced astrocyte–astrocyte interactions that appeared to recapitulate the chain-like clustering of glial scar formation.

Overlay images of GFAP and tubulin (not shown) consistently indicated an interaction between GFAP and tubulin. The results shown in Figure 6 indicated that dBcAMP-treated astrocytes cultured on nanofibrillar scaffolds did not change either the codependence (PC) or the overlap of GFAP and tubulin (M1 and M2). For all surfaces except nanofibrillar scaffolds, M1 and M2 coefficients significantly increased when they were treated with dBcAMP. The highest PC was observed for astrocytes cultured on Aclar surfaces,

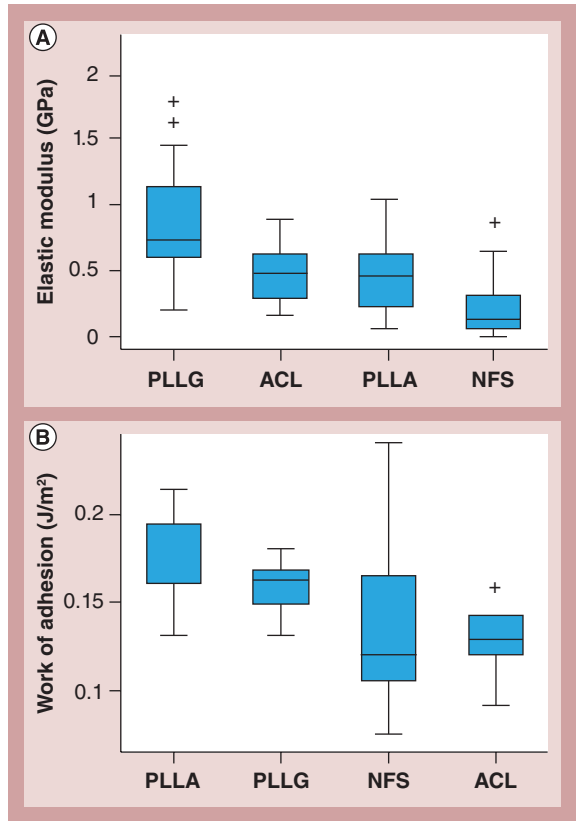

Figure 1. Elasticity and work of adhesion characterization of culture surfaces. (A) Young's modulus box plot. PLLG substrate is stiffer than other substrates. **(B)** Work of adhesion characterization of culture surfaces. PLL functionalization appears to increase the work of adhesion. Solid lines show the median, and the box edges show the 25th and 75th percentiles.
ACL: Aclar® (Ted Pella Inc., CA, USA); PLLA: Poly-L-lysine Aclar; PLLG: Poly-L-lysine glass; NFS: Nanofibrillar scaffolds.

10.2217/NNM.14.33

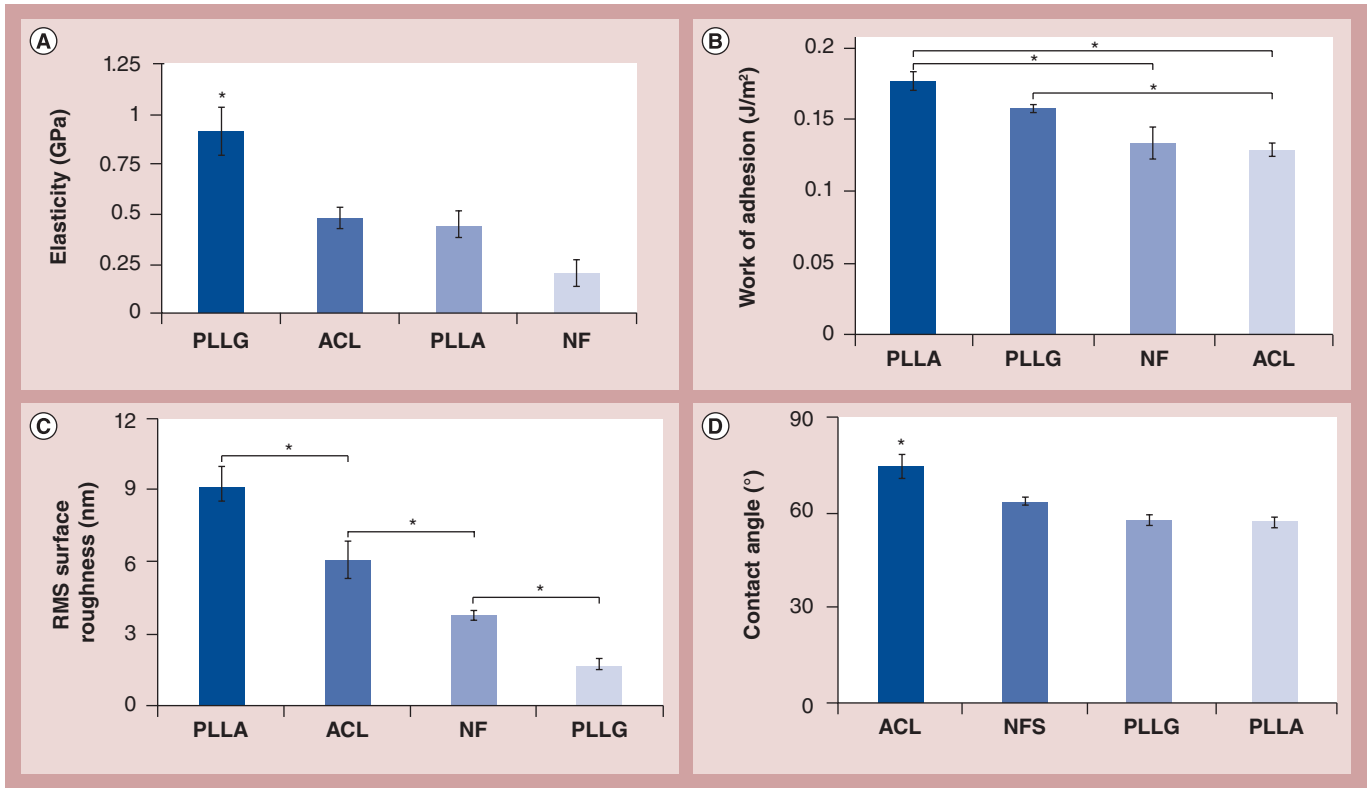

Figure 2. Physical properties of culture surfaces. (A) Elasticity, **(B)** work of adhesion, **(C)** surface roughness and **(D)** surface polarity. The error bars show the standard error of the mean. *p < 0.05.
ACL: Aclar® (Ted Pella Inc., CA, USA); NFS: Nanofibrillar scaffolds; PLLA: Poly-L-lysine Aclar; PLLG: Poly-L-lysine glass; RMS: Root mean squared.

for both untreated and dBcAMP-treated astrocytes, which indicated the highest codependence of GFAP and tubulin. Two-way ANOVA revealed that the PC, M1, and M2 coefficients were significantly influenced by both the substrates and by the dBcAMP treatment ($p < 0.05$).

CSPG quantification

Expressions of inhibitory proteoglycans CSPG for untreated and dBcAMP-treated astrocytes were analyzed and the results are shown in Figure 7. Both the substrate ($p < 0.001$) and dBcAMP treatment ($p = 0.0014$) were statistically significant factors. Results showed that the CSPG expressions of the dBcAMP-treated astrocytes significantly decreased relative to their untreated expressions for astrocytes cultured on the nanofibrillar scaffolds and Aclar surfaces.

Cdc42, Rac1 & RhoA quantification

The dBcAMP-treated astrocytes were immunolabeled by antibodies against Cdc42, Rac1 and RhoA, members of the Rho GTPase family, which are known to be upstream regulators of filopodia, lamellipodia and stress fiber formation, respectively [45]. For dBcAMP-treated astrocytes (Figure 8A), RhoA was depressed relative to Rac1 for all culture surfaces. This result is consistent with reactive process development through a depression of RhoA mechanism [46] in dBcAMP-treated astrocytes. For untreated astrocytes alone (Figure 8B), RhoA was significantly depressed relative to Cdc42 only for astrocytes cultured on the nanofibrillar scaffolds.

For dBcAMP-treated versus untreated astrocytes, Rho GTPase expressions for dBcAMP-treated astrocytes were shown to be modulated by the different

Table 1. Astrocyte density measurement results in cells/mm² (mean ± standard error of the mean).

Cells	PLL glass	Nanofibrillar scaffolds	Aclar	PLL aclar
dBcAMP-treated	189 ± 24	206 ± 14	177 ± 7	202 ± 17
Untreated	243 ± 26	186 ± 12	173 ± 12	252 ± 19

dBcAMP: Dibutyryladenosine cyclic monophosphate; PLL: Poly-L-lysine.

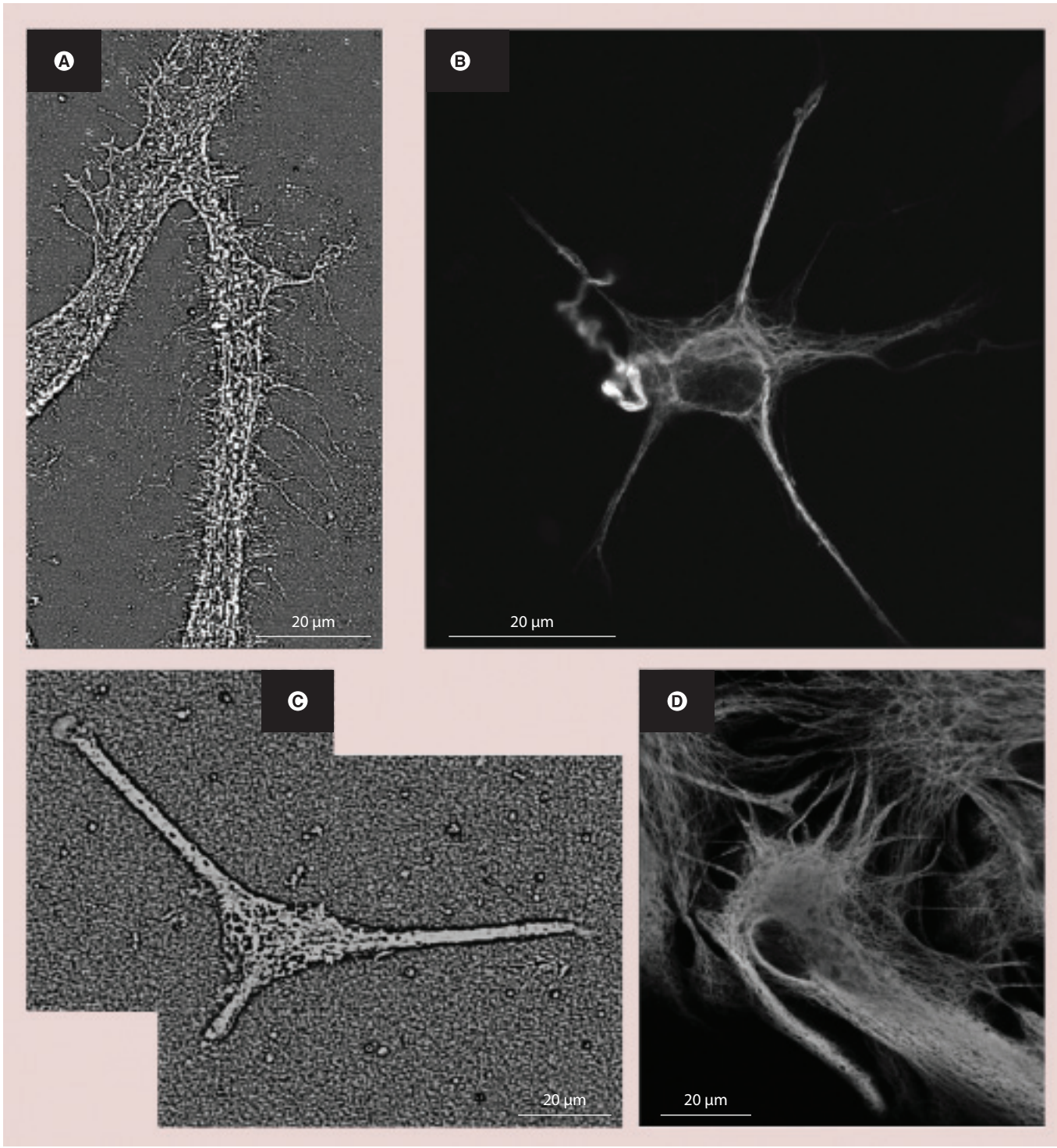

Figure 3. Morphology investigation of dibutyryladenosine cyclic monophosphate-treated astrocytes with (A & C) atomic force microscopy height Gaussian high pass filtering images and (B & D) super-resolution microscopy glial fibrillary acidic protein staining images. (A) Astrocytes cultured on poly-L-lysine glass formed numerous nanoscale processes. **(B)** Astrocytes cultured on nanofibrillar scaffolds have multiple stellate processes. Astrocytes cultured on **(C)** Aclar® (Ted Pella Inc., CA, USA) formed few directional processes, and ones on **(D)** poly-L-lysine Aclar formed overlapping processes.

10.2217/NNM.14.33

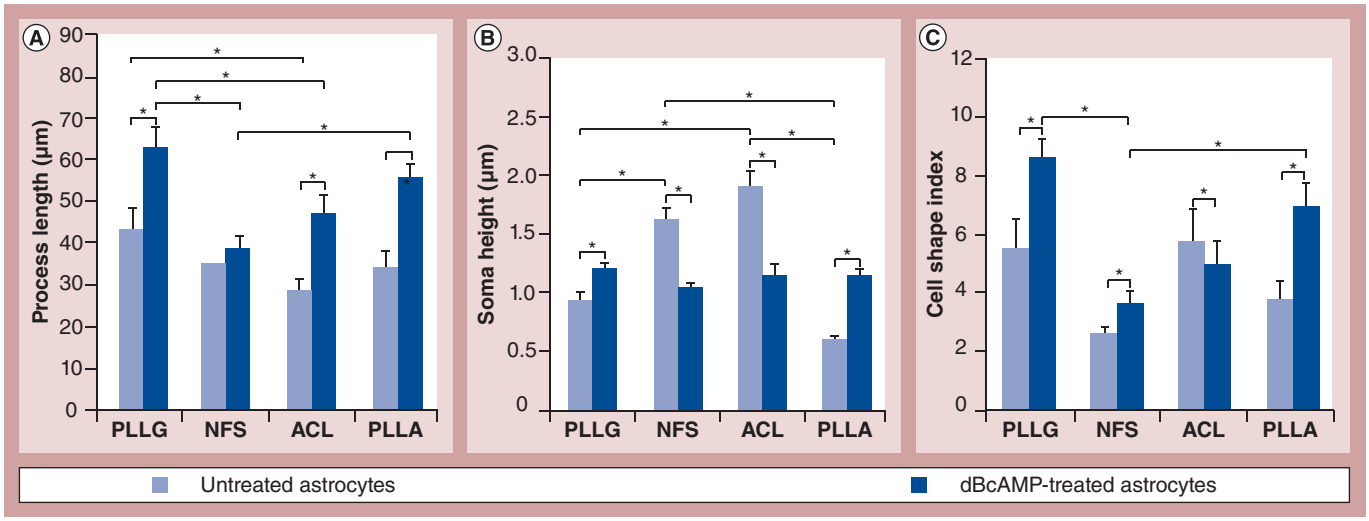

Figure 4. Atomic force microscopy-based quantitative morphology assessment of untreated and dibutyryladenosine cyclic monophosphate-treated astrocytes cultured on poly-L-lysine glass, nanofibrillar scaffolds, Aclar® (Ted Pella Inc., CA, USA) and poly-L-lysine Aclar. (A) Average length of astrocyte processes. **(B)** Average maximum soma height. **(C)** Average cell shape index results. NFS appear to control the immunoreactivity of astrocytes. The error bars show the standard error of the mean of n = 20 cells.
*p < 0.05.
ACL: Aclar® (Ted Pella Inc., CA, USA); dBcAMP: Dibutyryladenosine cyclic monophosphate; PLLA: Poly-L-lysine Aclar; PLLG: Poly-L-lysine glass; NFS: Nanofibrillar scaffolds.

culture surfaces (Figure 8A) in ways that differed from the modulation observed for untreated astrocytes (Figure 8B). Comparison of Figures 8A & 8B showed that the dBcAMP treatment of astrocytes reversed the relative expression of Cdc42, Rac1, and RhoA on all culture surfaces, except for the nanofibrillar scaffolds.

Discussion

The present study demonstrated that the physical properties of nanofibrillar scaffolds uniquely influenced the differentiation of dBcAMP-treated astrocytes. Quantitative investigation showed that process lengths for dBcAMP-treated astrocytes were the same to within

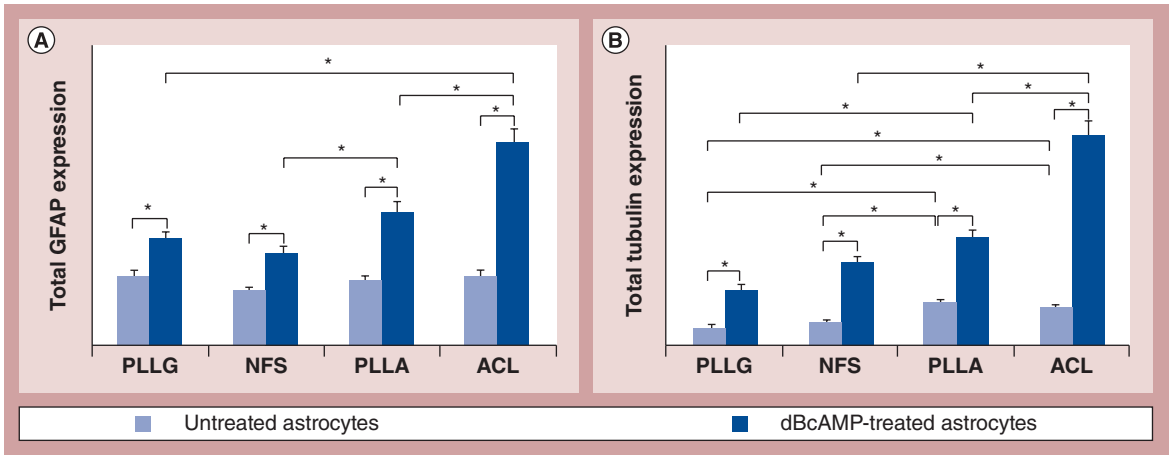

Figure 5. Quantitative total (A) glial fibrillary acidic protein and (B) tubulin expression estimate for untreated and dibutyryladenosine cyclic monophosphate-treated astrocytes. The dBcAMP-treated astrocytes on NFS produced significantly less GFAP than ones on PLLA and ACL, and less tubulin than ones on ACL. Error bars show the standard error of the mean of n = 50 astrocytes. The quantitative total GFAP expression estimate is a relative intensity measurement. The value range for total GFAP expression is 400% when the total GFAP expression of untreated astrocyte on PLLG (shown on the very left side of **[A]**) is assumed to be 100% (intensities are scaled to untreated PLLG = 100%). This is similar for the total tubulin expression. The value range for total tubulin expression is 1500% when the total tubulin expression of untreated astrocytes on PLLG (shown on the very left side of **[B]**) is assumed to be 100% (intensities are scaled to untreated PLLG = 100%).
*p < 0.05.
ACL: Aclar® (Ted Pella Inc., CA, USA); dBcAMP: Dibutyryladenosine cyclic monophosphate; GFAP: Glial fibrillary acidic protein; PLLA: Poly-L-lysine Aclar; PLLG: Poly-L-lysine glass; NFS: Nanofibrillar scaffolds.

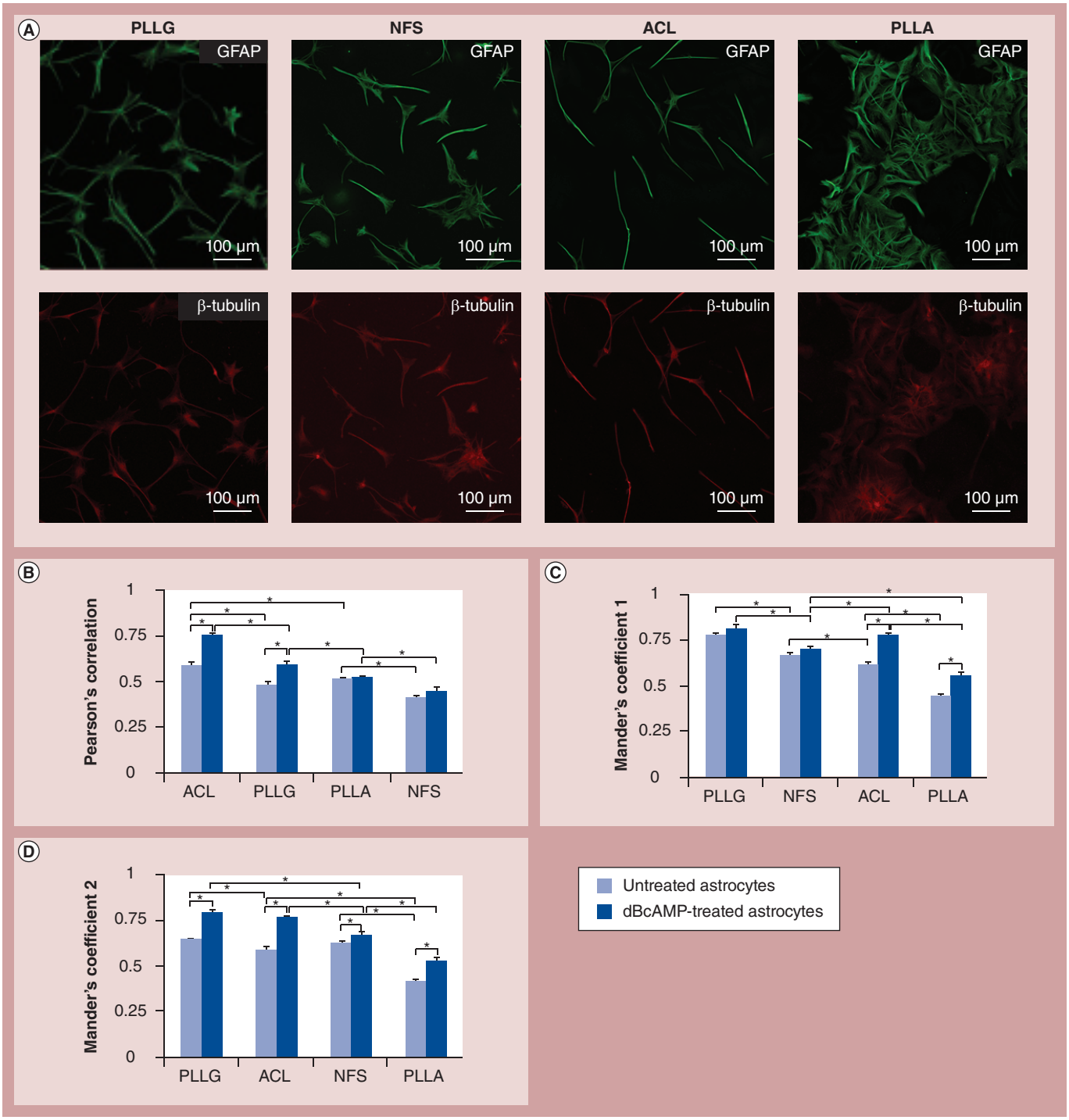

Figure 6. Maximum intensity projection glial fibrillary acidic protein and tubulin staining images of dibutyryladenosine cyclic monophosphate-treated astrocytes cultured on poly-L-lysine glass, nanofibrillar scaffolds, Aclar® (Ted Pella Inc., CA, USA) and poly-L-lysine Aclar. (A) Astrocytes on PLLA surfaces formed chain-like glial scar formation while astrocytes on NFS and the other surfaces were not clustered. **(B–D)** Colocalization analysis results based on 3D GFAP and tubulin immunofluorescence images. Pearson's correlations of untreated and dBcAMP-treated astrocytes were significantly different for all surfaces except ones on NFS and PLLA. Mander's coefficient M1 of untreated and dBcAMP-treated astrocytes were significantly different for all surfaces except for astrocytes cultured on NFS and PLLG. Error bars show the standard error of the mean of n = 10 coefficient values measured from confocal z-series.

*$p < 0.05$.

ACL: Aclar® (Ted Pella Inc., CA, USA); dBcAMP: Dibutyryladenosine cyclic monophosphate; GFAP: Glial fibrillary acidic protein; PLLA: Poly-L-lysine Aclar; PLLG: Poly-L-lysine glass; NFS: Nanofibrillar scaffolds.

10.2217/NNM.14.33

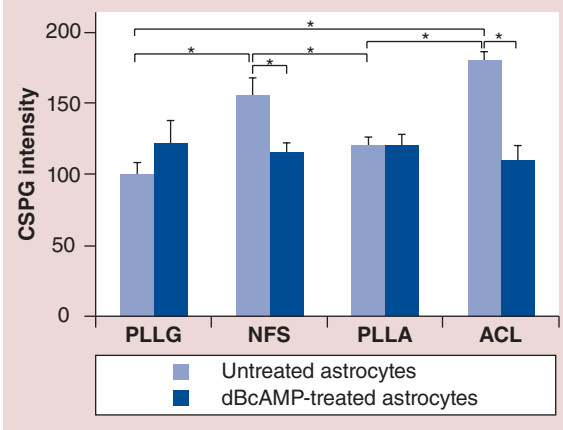

Figure 7. Quantitative chondroitin sulfate proteoglycan expression estimation results. NFS and ACL surfaces significantly reduced CSPG expression when the astrocytes were treated with dBcAMP. Error bars show the standard error of the mean of n = 12 confocal z-series.
*p < 0.05.
ACL: Aclar® (Ted Pella Inc., CA, USA); CSPG: Chondroitin sulfate proteoglycan; dBcAMP: Dibutyryladenosine cyclic monophosphate; PLLA: Poly-L-lysine Aclar; PLLG: Poly-L-lysine glass; NFS: Nanofibrillar scaffolds.

statistical error as those for untreated astrocytes. This is consistent with RhoA results that indicated that untreated astrocytes on the nanofibrillar scaffolds showed evidence of stellation via a RhoA depression mechanism, which did not change for the dBcAMP-treated astrocytes. As a consequence, the dBcAMP-treated astrocytes adopted *in vivo* like stellate morphologies on the nanofibrillar scaffolds (Figure 3B) that were similar to those observed for untreated astrocytes [12]. The dBcAMP-treated and untreated pairwise comparisons further showed that dBcAMP-treated astrocytes on the comparative culture surfaces all developed significantly longer processes, with the exception of the ones cultured on the nanofibrillar scaffolds.

Pairwise comparisons of dBcAMP-treated and untreated astrocytes indicated a statistical increase in GFAP expression on all culture surfaces. However, the dBcAMP-treated astrocytes cultured on the nanofibrillar scaffolds had significantly lower expression of GFAP than PLL Aclar and Aclar, and no statistically significant difference of GFAP expression on PLL glass. The dBcAMP-treated astrocytes on the nanofibrillar scaffolds had significantly lower expression of tubulin than on Aclar, and no statistical differences on PLL glass and PLL Aclar. When colocalization of GFAP and tubulin was considered, pairwise comparison of untreated and dBcAMP-treated astrocytes showed that astrocytes on nanofibrillar scaffolds have statistically unchanged PC and M1 coefficients and the lowest increase in M2 coefficient. This indicates that the association of GFAP with tubulin was relatively unchanged for dBcAMP-treated astrocytes on nanofibrillar scaffolds. By contrast, pairwise comparisons showed that the either PC or M1 of the dBcAMP-treated astrocytes on the comparative culture surfaces all significantly increased, in addition to larger increases in M2. These results indicate that interaction with the nanofibrillar scaffolds reduced the reactivity of astrocytes.

Pairwise comparisons of dBcAMP-treated and untreated astrocytes indicated a statistically significant decrease in expression of CSPG on nanofibrillar scaffolds and on Aclar. The cell density measurements of Table 1 suggested that the observed CSPG level decrease on Aclar might be linked to a decrease in astrocyte numbers for the dBcAMP-treated astrocytes. Astrocyte numbers for the dBcAMP-treated astrocytes on the nanofibrillar scaffolds were the highest observed. This indicates that the interaction with the nanofibrillar scaffolds modulated the observed decreased CSPG expression.

In sharp contrast to the minimal changes and reduction in immunoreactivity responses displayed by dBcAMP-treated astrocytes on the nanofibrillar scaffolds, the responses to PLL Aclar exhibited features reminiscent of glial scar formation. Chain-like clustering of dBcAMP-treated astrocytes with interwoven processes was evident in immunostaining (Figure 6), AFM (not shown), and SRM images (Figure 3D). Pairwise comparisons of dBcAMP-treated and untreated astrocytes showed that the most statistically significant increase in process lengths for dBcAMP-treated astrocytes on PLL Aclar surfaces. In pairwise comparisons of dBcAMP-treated and untreated astrocytes only the dBcAMP-treated astrocytes on PLL Aclar showed a statistically unchanged PC with statistically significant increases in M1 and M2. This indicates that the codependence of GFAP and tubulin did not change but their overlap increased. The immunoreactivity investigation indicated high expressions of both GFAP and tubulin by dBcAMP-treated astrocytes on PLL Aclar. In terms of significance, the GFAP expression was significantly higher than on nanofibrillar scaffolds and the tubulin expression was significantly higher than on PLL glass. The CSPG expression was statistically unchanged in pairwise comparisons of dBcAMP-treated and untreated astrocytes. The greatest changes were therefore observed in proteins associated with morphological responses.

In the present work, the effects of culture surface physical properties on the morphological and biochemical differentiation of dBcAMP-treated cerebral cortical astrocytes (rat model) were investigated *in vitro*. Four physical properties of the culture surfaces were considered as potentially directive: elasticity,

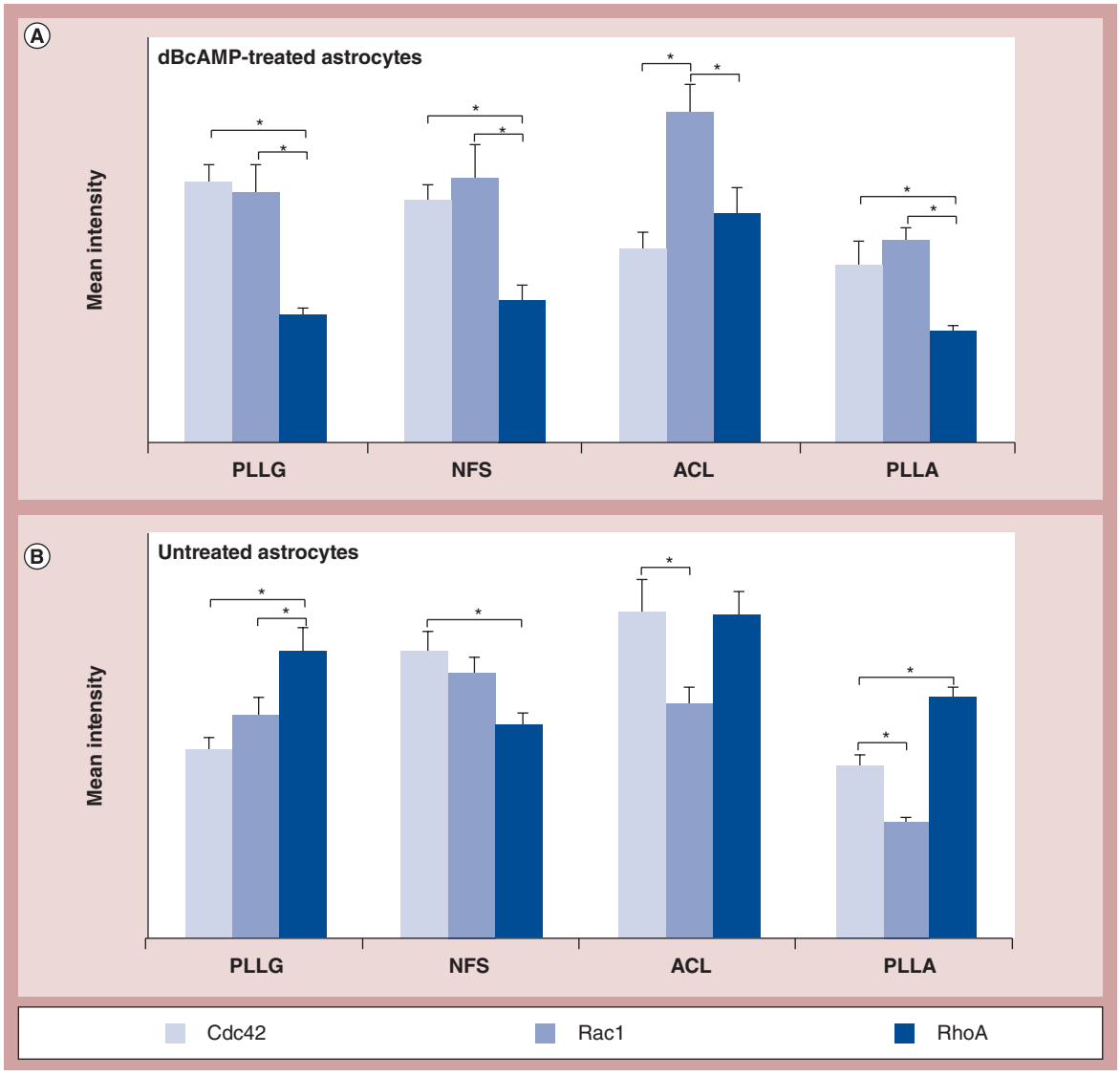

Figure 8. Quantitative Cdc42, Rac1 and RhoA expression estimation results for (A) reactive-like and (B) quiescent astrocytes. Error bars show the standard error of the mean of n = 20 cells.
*$p < 0.05$.
ACL: Aclar® (Ted Pella Inc., CA, USA); dBcAMP: Dibutyryladenosine cyclic monophosphate; PLLA: Poly-L-lysine Aclar; PLLG: Poly-L-lysine glass; NFS: Nanofibrillar scaffolds.
(B) Reproduced with permission from [12].

work of adhesion, surface polarity and surface roughness. The results demonstrated that the morphological and biochemical differentiation of untreated and dBcAMP-treated astrocytes were modulated by the physical properties of the culture surfaces. Comparison of dBcAMP-treated versus untreated responses further demonstrated that the responses were differently modulated by the same culture surface properties.

In our previous study [12], untreated astrocytes on PLL Aclar surfaces developed extensive filopodia formation that infiltrated along valleys created by the nanoscale surface roughness of these surfaces, a response that was not observed on the nanoscale-smooth PLL glass surfaces. For the dBcAMP-treated astrocytes in the present study, a glial scar type response was observed instead of filopodia formation on the same PLL Aclar surfaces. The physical property investigations summarized in Figure 2 demonstrated that statistically significant elasticity differences were present between the PLL glass and other culture surfaces. Previously reported results [47–49] have indicated increased sensitivity to local elasticity as a response to wound-healing situations. Additionally, comparisons of dBcAMP-treated astrocytes responses on PLL Aclar versus Aclar showed that the surface energy property appeared to be directive. Significantly different reactivity protein

10.2217/NNM.14.33

expressions (Figures 5 & 6) and morphological responses (Figure 3) were observed.

The chain-like clustering of dBcAMP-treated astrocytes appeared to be induced by the local elastic property of the PLL Aclar surface in combination with the surface energy property. The directive nature of the elasticity property was indicated by the chain-like versus non-chain-like clustering observed for dBcAMP-treated astrocytes on PLL Aclar (softer) versus PLL glass (harder). The directive nature of the surface polarity in combination with the elasticity property was indicated by the chain-like clustering versus the unusual morphology and minimal cell–cell interactions observed for dBcAMP-treated astrocytes on PLL Aclar (softer elasticity and higher hydrophilicity) versus Aclar (softer elasticity and lowest hydrophilicity) (Figure 2). Studies of hydrogel-assisted wound healing [49] further suggest that the combination of local elasticity and surface charge may be directive, which is consistent with our reported results. Chain-like clustering was not observed on the nanofibrillar scaffolds (softer elasticity). Macroscopic contact angle measurements did not indicate any surface polarity difference between the nanofibrillar scaffolds and PLL Aclar (Figure 2); however, the nanoscopic work of adhesion measurements indicated statistical differences in surface energy were present at a local (focal adhesion scale) level. While further investigations into the mechanisms that are responsible for the observed beneficial effects of nanofibrillar scaffolds are necessary, this suggests that the local environment may be important.

The property investigations and corresponding astrocyte *in vitro* behavior in the present study showed that a combination of tissue scaffold physical properties can modulate cellular mechanisms of dBcAMP-treated astrocytes. This suggests that scaffolds with appropriate physical properties could alter the immunoreactivity of astrocytes, which may promote axonal regeneration around a lesion site. The polyamide nanofibrillar scaffolds appear to have the optimum physical properties among the culture surfaces considered in this work. Therefore, it remains as a promising candidate for future *in vivo* investigations.

Conclusion

The morphological and biochemical differentiation of dBcAMP-treated astrocytes cultured on electrospun polyamide nanofibrillar scaffolds, PLL glass, Aclar and PLL Aclar was investigated by immunocytochemistry, colocalization, SRM and AFM. Four physical properties of the culture surfaces were considered as potentially directive: elasticity, work of adhesion, surface polarity and surface roughness. The physical properties of the culture environment were shown to trigger biochemical and morphological consequences for dBcAMP-treated astrocytes. The properties of the nanofibrillar scaffolds appear to reduce immunoreactivity responses while the properties of the PLL Aclar surfaces induced responses reminiscent of glial scar formation. The comparison of dBcAMP-treated and untreated astrocyte responses suggested that different nanophysical cues may have more directive importance in a wound-healing situation than in a maintenance situation. Local elasticity and surface polarity were indicated as potentially directive for dBcAMP-treated cerebral cortical astrocytes.

Future perspective

Results from this research are likely to have a major impact on regenerative medicine aimed at recreating the neural cell system following CNS injury. This is one of the most intractable injury situations, with no cure for the para- or quadra-plegia that results from severe injuries. Furthermore, as cell systems that are influences by scaffold-based environments are ubiquitous throughout the body, identification of the fundamental set of nanoscale properties that promote healthy neural cell physiology and function serves as the basis for the quantitative exploration of other regenerative cell-scaffold systems. In addition to regenerative medicine, quantitative investigation of the nanoscale cues that direct cell–cell interactions will also advance such diverse fields as stem cell and cancer research.

Financial & competing interests disclosure

The support of National Science Foundation grants PHY-0957776 (VM Ayres and VM Tiryaki), ARRA-CBET-0846328 (DI Shreiber and I Ahmed) and the General Directorate for Higher Education, Ministry of National Education of the Republic of Turkey (VM Tiryaki) are gratefully acknowledged. The authors thank M Frame (Michigan State University, MI, USA) for valuable discussions about quantitative immunolabeling analysis, and A Tirrell (Michigan State University) for her assistance in imaging the atomic force microscopy probe with field emission scanning electron microscopy. The authors have no other relevant affiliations or financial involvement with any organization or entity with a financial interest in or financial conflict with the subject matter or materials discussed in the manuscript apart from those disclosed.

No writing assistance was utilized in the production of this manuscript.

Ethical conduct of research

The authors state that they have obtained appropriate institutional review board approval or have followed the principles outlined in the Declaration of Helsinki for all human or animal experimental investigations.

Executive summary

Astrocyte responses to nanophysical properties

- The nanophysical properties of four culture environments were shown to trigger biochemical and morphological consequences for dibutyryladenosine cyclic monophosphate (dBcAMP)-treated astrocytes. Properties characterized and considered were: nanoscopic elasticity, work of adhesion, surface roughness and macroscopic surface polarity.
- The properties of a promising nanofibrillar scaffold environment were shown to reduce immunoreactivity and inhibitory proteoglycan responses while the properties of a poly-L-lysine (PLL) Aclar® (Ted Pella Inc., CA, USA) environment were shown to induce responses reminiscent of glial scar formation. Statistically unchanged Rho GTPase expressions were uniquely observed for dBcAMP-treated astrocytes on the nanofibrillar scaffolds.
- Responses of dBcAMP-treated astrocytes were compared with our 2012 investigation of untreated astrocytes responses to the same environments/properties, and indicated that different nanophysical cues may have more directive importance in wound-healing situations versus maintenance situations.
- Quantitative investigations of immunoreactivity protein expressions were performed for dBcAMP-treated astrocytes. Quantitative investigations and comparisons of Rho GTPase protein expressions were performed for dBcAMP-treated and untreated astrocytes. Astrocytes on nanofibrillar scaffolds had unique, minimally changed Rho GTPase protein expressions.
- Quantitative investigations of morphological features: process length, cell spreading and cell shape index were performed for dBcAMP-treated and untreated astrocytes. Astrocytes on nanofibrillar scaffolds had unique, minimally changed morphological responses.
- The present work contributes quantitative investigations to an integrated physics–biology research area that is attracting increasing attention: the regulation of cell responses by topographical cues at the nano level.

Nanophysical property measurements

- Elasticity characterization of culture surfaces showed statistically significant differences between PLL glass, Aclar and nanofibrillar scaffolds. Nanofibrillar scaffolds were softest. Work of adhesion characterization was consistent with the macroscopic surface polarity of culture surfaces.

References

Papers of special note have been highlighted as:
• of interest
•• of considerable interest

1 Sivron T, Schwartz M. Glial-cell types, lineages, and response to injury in rat and fish – implications for regeneration. *Glia* 13(3), 157–165 (1995).

2 Ridet JL, Malhotra SK, Privat A, Gage FH. Reactive astrocytes: cellular and molecular cues to biological function. *Trends Neurosci.* 20(12), 570–577 (1997).

3 Wilhelmsson U, Bushongt EA, Price DL *et al.* Redefining the concept of reactive astrocytes as cells that remain within their unique domains upon reaction to injury. *Proc. Natl Acad. Sci. USA* 103(46), 17513–17518 (2006).

4 Wiese S, Karus M, Faissner A. Astrocytes as a source for extracellular matrix molecules and cytokines. *Front. Pharmacol.* 3, 120 (2012).

5 Silver J, Miller JH. Regeneration beyond the glial scar. *Nat. Rev. Neurosci.* 5(2), 146–156 (2004).

6 Zhou K, Nisbet D, Thouas G, Bernard C, Forsythe J. *Bio-nanotechnology Approaches to Neural Tissue Engineering.* InTech, NY, USA, 459–484 (2010).

7 Meiners S, Harris S, Delgado-Rivera R *et al. A Nanofibrillar Prosthetic Modified with Fibroblast Growth Factor-2 for Spinal Cord Repair.* Nova Science Publishers Inc., NY, USA, 327–343 (2009).

•• **Promising *in vivo* results for successful spinal cord wound repair using polyamide nanofibrillar scaffolds, which included documentation by standard Beattie, Basso, Breshnahan observational scoring, were demonstrated in this work.**

8 Meiners S, Ahmed I, Ponery AS *et al.* Engineering electrospun nanofibrillar surfaces for spinal cord repair: a discussion. *Polym. Int.* 56(11), 1340–1348 (2007).

9 Delgado-Rivera R, Harris SL, Ahmed I *et al.* Increased FGF-2 secretion and ability to support neurite outgrowth by astrocytes cultured on polyamide nanofibrillar matrices. *Matrix Biol.* 28(3), 137–147 (2009).

•• **Promising *in vitro* results for successful modulation of cerebral cortical astrocytes by polyamide nanofibrillar scaffolds were demonstrated in this work. Astrocytes assumed stellate morphologies, demonstrated autocrine upregulation of FGF-2 growth factor and were more permissive for neurite outgrowth of cocultured neurons compared with standard planar culture surfaces.**

10 Puschmann TB, Zanden C, De Pablo Y *et al.* Bioactive 3D cell culture system minimizes cellular stress and maintains the *in vivo*-like morphological complexity of astroglial cells. *Glia* 61(3), 432–440 (2013).

11 Min SK, Kim CR, Jung SM, Shin HS. Astrocyte behavior and GFAP expression on Spirulina extract-incorporated PCL nanofiber. *J. Biomed. Mater. Res. A* 101(12), 3467–3473 (2013).

12 Tiryaki VM, Ayres VM, Khan AA, Ahmed I, Shreiber DI, Meiners S. Nanofibrillar scaffolds induce preferential activation of Rho GTPases in cerebral cortical astrocytes. *Int. J. Nanomed.* 7, 3891–3905 (2012).

•• **Fundamental study in support of the hypothesis that the extracellular environment can trigger preferential**

10.2217/NNM.14.33

activation of members of the Rho GTPase family with demonstrable morphological consequences for untreated cerebral cortical astrocytes.

13 Vignaud T, Galland R, Tseng QZ, Blanchoin L, Colombelli J, Thery M. Reprogramming cell shape with laser nano-patterning. *J. Cell Sci.* 125(9), 2134–2140 (2012).

14 Koegler P, Clayton A, Thissen H, Santos GNC, Kingshott P. The influence of nanostructured materials on biointerfacial interactions. *Adv. Drug Deliver. Rev.* 64(15), 1820–1839 (2012).

15 Yim EKF, Pang SW, Leong KW. Synthetic nanostructures inducing differentiation of human mesenchymal stem cells into neuronal lineage. *Exp. Cell Res.* 313(9), 1820–1829 (2007).

16 Wood JA, Ly I, Borjesson DL, Nealey PF, Russell P, Murphy CJ. The modulation of canine mesenchymal stem cells by nano-topographic cues. *Exp. Cell Res.* 318(19), 2438–2445 (2012).

17 Ahmed I, Ponery AS, Nur-E-Kamal A *et al.* Morphology, cytoskeletal organization, and myosin dynamics of mouse embryonic fibroblasts cultured on nanofibrillar surfaces. *Mol. Cell. Biochem.* 301(1–2), 241–249 (2007).

18 Georges PC, Miller WJ, Meaney DF, Sawyer ES, Janmey PA. Matrices with compliance comparable to that of brain tissue select neuronal over glial growth in mixed cortical cultures. *Biophys. J.* 90(8), 3012–3018 (2006).

•• **One of the first studies to demonstrate the durotactic response of cortical neurons and astrocytes to variations in matrix stiffness.**

19 Engler AJ, Sen S, Sweeney HL, Discher DE. Matrix elasticity directs stem cell lineage specification. *Cell* 126(4), 677–689 (2006).

20 Nemir S, West JL. Synthetic materials in the study of cell response to substrate rigidity. *Ann. Biomed. Eng.* 38(1), 2–20 (2010).

21 Leipzig ND, Shoichet MS. The effect of substrate stiffness on adult neural stem cell behavior. *Biomaterials* 30(36), 6867–6878 (2009).

22 Banerjee A, Arha M, Choudhary S *et al.* The influence of hydrogel modulus on the proliferation and differentiation of encapsulated neural stem cells. *Biomaterials* 30(27), 4695–4699 (2009).

23 Jiang FX, Yurke B, Firestein BL, Langrana NA. Neurite outgrowth on a DNA crosslinked hydrogel with tunable stiffnesses. *Ann. Biomed. Eng.* 36(9), 1565–1579 (2008).

24 Hallab NJ, Bundy KJ, O'connor K, Moses RL, Jacobs JJ. Evaluation of metallic and polymeric biomaterial surface energy and surface roughness characteristics for directed cell adhesion. *Tissue Eng.* 7(1), 55–71 (2001).

• **The authors identify the relationship between the surface roughness and surface energy of scaffolds and their influence on cell adhesion.**

25 Tonazzini I, Bystrenova E, Chelli B *et al.* Multiscale morphology of organic semiconductor thin films controls the adhesion and viability of human neural cells. *Biophys. J.* 98(12), 2804–2812 (2010).

26 Biran R, Noble MD, Tresco PA. Characterization of cortical astrocytes on materials of differing surface chemistry. *J. Biomed. Mater. Res.* 46(2), 150–159 (1999).

27 Fedoroff S, Mcauley WaJ, Houle JD, Devon RM. Astrocyte cell lineage. 5. Similarity of astrocytes that form in the presence of dBcAMP in cultures to reactive astrocytes *in vivo*. *J. Neurosci. Res.* 12(1), 15–27 (1984).

28 Petroski RE, Grierson JP, Choikwon S, Geller HM. Basic fibroblast growth-factor regulates the ability of astrocytes to support hypothalamic neuronal survival *in vitro*. *Dev. Biol.* 147(1), 1–13 (1991).

29 Tiryaki VM, Khan AA, Ayres VM. AFM feature definition for neural cells on nanofibrillar tissue scaffolds. *Scanning* 34(5), 316–324 (2012).

30 Spatz C. *Basic Statistics: Tales of Distributions*. Cengage Learning, CT, USA (2011).

31 East E, Golding JP, Phillips JB. A versatile 3D culture model facilitates monitoring of astrocytes undergoing reactive gliosis. *J. Tissue Eng. Regen. Med.* 3(8), 634–646 (2009).

32 Tiryaki V, Adia-Nimuwa U, Hartz S *et al.* New atomic force microscopy based astrocyte cell shape index. *MRS Proc.* 1527, (2012).

33 Matsutani S, Yamamoto N. Neuronal regulation of astrocyte morphology *in vitro* is mediated by GABAergic signaling. *Glia* 20(1), 1–9 (1997).

34 Hopcroft MA, Nix WD, Kenny TW. What is the Young's modulus of silicon? *J. Microelectromech. Syst.* 19(2), 229–238 (2010).

35 Derjaguin BV, Muller VM, Toporov YP. Effect of contact deformations on the adhesion of particles. *Prog. Surf. Sci.* 45(1–4), 131–143 (1994).

36 Jogikalmath G, Stuart JK, Pungor A, Hlady V. Adhesion mapping of chemically modified and poly(ethylene oxide)-grafted glass surfaces. *Colloids Surf. A Physicochem. Eng. Asp.* 154(1–2), 53–64 (1999).

37 Khan A, Philip J, Hess P. Young's modulus of silicon nitride used in scanning force microscope cantilevers. *J. Appl. Phys.* 95(4), 1667–1672 (2004).

38 Greaves GN, Greer AL, Lakes RS, Rouxel T. Poisson's ratio and modern materials. *Nat. Mater.* 10, 823–837 (2011).

39 Rouxel T. Elastic properties and short-to medium-range order in glasses. *J. Am. Ceram. Soc.* 90(10), 3019–3039 (2007).

40 Greaves GN, Greer AL, Lakes RS, Rouxel T. Poisson's ratio and modern materials. *Nat. Mater.* 10(11), 823–837 (2011).

41 Coleman TF, Li YY. An interior trust region approach for nonlinear minimization subject to bounds. *SIAM J. Optimiz.* 6(2), 418–445 (1996).

42 Bolte S, Cordelieres FP. A guided tour into subcellular colocalization analysis in light microscopy. *J. Microsc.* 224(Pt 3), 213–232 (2006).

43 Lin DC, Dimitriadis EK, Horkay F. Robust strategies for automated AFM force curve analysis-II: adhesion-influenced indentation of soft, elastic materials. *J. Biomech. Eng.* 129(6), 904–912 (2007).

44 Dreher Z, Tout S, Stone J. Interactions of living astrocytes *in vitro* – evidence of the development of contact spacing. *Glia* 11(1), 57–63 (1994).

45 Nobes CD, Hall A. Rho, Rac, and Cdc42 Gtpases regulate the assembly of multimolecular focal complexes associated with actin stress fibers, lamellipodia, and filopodia. *Cell* 81(1), 53–62 (1995).

46 Abe K, Misawa M. Astrocyte stellation induced by Rho kinase inhibitors in culture. *Dev. Brain Res.* 143(1), 99–104 (2003).

• **Showed that the stellation of astrocytes can be induced by Rho kinase inhibitors.**

47 Georges P, Mccormick M, Flanagan L, Ju Y, Sawyer E, Janmey P. Tuning the elasticity of biopolymer gels for optimal wound healing. *MRS Proc.* 897, (2005).

48 Taber LA. Towards a unified theory for morphomechanics. *Philos. Trans Math. Phys. Eng. Sci.* 367 (1902), 3555–3583 (2009).

49 Zuidema JM, Pap MM, Jaroch DB, Morrison FA, Gilbert RJ. Fabrication and characterization of tunable polysaccharide hydrogel blends for neural repair. *Acta Biomater.* 7(4), 1634–1643 (2011).

10.2217/NNM.14.33